PAPER

Check for updates

Silk fibroin scaffolds loaded with growth factors can reverse liver fibrosis

Jingyi Wang,†[a] Zhanbo Wang,†[b] Shuo Zhao,†[c] Daxu Zhang,[a] Jingjing Hu,[a] Weilong Li,[a] Xiaonan Shi,[a] Shujun Ye,[a] Xiaojiao Liu,[d] Yaopeng Zhang [ID] *[d] and Li Yan [ID] *[a]

Currently, there are no effective pharmacological interventions in clinical practice to reverse liver fibrosis. This study explores the therapeutic potential of regenerated silk fibroin (RSF) scaffolds loaded with dual growth factors for reversing hepatic fibrosis. A chronic liver fibrosis mouse model was induced using carbon tetrachloride (CCl_4) combined with a high-fat diet. RSF scaffolds, with or without hepatocyte growth factor (HGF) and fibroblast growth factor-4 (FGF-4), were implanted onto the liver surface to assess antifibrotic efficacy. Liver function was evaluated using biochemical analysis. Compared with controls, the RSF/HGF/FGF-4 group showed significantly reduced serum levels of C-reactive protein (CRP), alanine aminotransferase (ALT), and aspartate aminotransferase (AST). Histopathological analyses (H&E and Masson's trichrome staining) on days 7, 14, and 30 demonstrated marked improvements in liver architecture and a significant reduction in fibrosis (SAF scores, $P < 0.05$). Immunohistochemistry further revealed neovascularization and bile duct formation by day 14. Transcriptomic profiling showed upregulation of bile duct development pathways and downregulation of inflammatory signaling. Quantitative PCR confirmed increased expression of bile secretion genes (FXR, OAT) and decreased expression of NF-κB pathway genes (TRAF2, Bax). These findings highlight the RSF/HGF/FGF-4 scaffold as a promising cell-free strategy for promoting functional liver regeneration and reversing chronic liver fibrosis.

1. Introduction

The liver plays an essential role in metabolic regulation and detoxification, and its functional integrity is critical for maintaining overall health and quality of life. Globally, the number of individuals affected by chronic liver disease has surpassed 800 million.[1] According to the Global Burden of Disease report, approximately 112 million patients have progressed to compensated cirrhosis, while 10.6 million have reached the decompensated stage. Liver cirrhosis-related mortality has risen to 1.32 million deaths, accounting for 2.4% of all deaths worldwide. As a country bearing high disease burden, China accounts for 27.8% of global cirrhosis-related deaths.[2–4]

[a]Department of Gastroenterology, Institute of Geriatrics, Chinese PLA General Hospital, No. 28 Fuxing Road, Haidian District, Beijing 100853, China. E-mail: yanlitg@163.com; Tel: +86 13671169179
[b]Department of Pathology, the First Medical Center, Chinese PLA General Hospital, No. 28 Fuxing Road, Haidian District, Beijing 100853, China
[c]Department of Critical Care Medicine, Aerospace Central Hospital, No. 15 Yuquan Road, Haidian District, Beijing 100083, China
[d]State Key Laboratory of Advanced Fiber Materials, College of Materials Science and Engineering, Donghua University, 2999 North Renmin Road, Songjiang District, Shanghai 201620, China. E-mail: zyp@dhu.edu.cn
† These authors contributed equally to this work.

Hepatic fibrosis, an inevitable intermediate stage in the progression from chronic liver disease to cirrhosis, remains a major therapeutic challenge due to the lack of effective pharmacological interventions. Consequently, developing strategies that can effectively reverse fibrosis and prevent its progression to cirrhosis has become an urgent medical priority.

In recent years, transplantation of adipose-derived stem cells (ADSCs) or bone marrow-derived mesenchymal stem cells (BM-MSCs) has emerged as a research hotspot in the treatment of hepatic fibrosis due to their regenerative and tissue repair potential.[5–8] Evidence suggests that the therapeutic effects of stem cell transplantation are primarily mediated by paracrine mechanisms that facilitate liver regeneration.[9] However, several critical limitations hinder the clinical translation of this approach, including low engraftment efficiency within hepatic tissue, the risk of embolism, and the necessity for repeated injections. These issues not only elevate treatment costs but also increase medical risks, significantly limiting its widespread clinical applicability.[10]

To overcome these limitations, HGF and FGF-4 have drawn increasing attention as alternative therapeutic agents for hepatic fibrosis. These growth factors replicate the reparative functions of stem cell-derived paracrine factors while avoiding the risks associated with cell transplantation. HGF, by activat-

ing the Met signaling pathway, effectively suppresses hepatic stellate cell activation and promotes hepatocyte proliferation,[11] at the same time, FGF-4 modulates extracellular matrix metabolism through the FGFR2 pathway. Both factors have been shown to significantly reduce collagen deposition in experimental fibrosis models.[12] Furthermore, the direct delivery of growth factors *via* RSF scaffolds eliminates the need for cell transplantation, thereby avoiding associated challenges such as poor engraftment efficiency and potential immune rejection. This scaffold-based approach offers a novel and promising therapeutic strategy for the treatment of hepatic fibrosis.

However, a major challenge in combining HGF and FGF-4 with scaffolds lies in balancing extracellular matrix (ECM) biomimicry with controlled release of bioactive factors. Although existing hydrogels and nanofibrous scaffolds have demonstrated certain therapeutic benefits in liver injury models, they are often limited by mismatched degradation-release kinetics and insufficient ECM mimicry.[13–15] Electrospun RSF nanofiber scaffolds exhibit distinct advantages due to their biomimetic structure (fiber diameter 500–2000 nm), high surface area (promoting cell adhesion and recruitment), and potential for sustained release of therapeutic agents and growth factors. Previous studies have shown that in a murine acute liver injury model, the RSF/HGF/FGF-4 group exhibited significantly lower SAF scores than the RSF-only group two days post-implantation.[16] Moreover, RSF combined with ADSCs has been shown to reverse chronic hepatic fibrosis, with liver function nearly restored by day 60.[17,18] Nonetheless, the therapeutic effects and underlying mechanisms of HGF- and FGF-4-loaded RSF scaffolds in chronic hepatic fibrosis remain unclear. Specifically, it is yet to be studied whether these scaffolds exert their antifibrotic effects through inhibition of hepatic stellate cell activation *via* modulation of the TGF-β/Smad signaling pathway, upregulation of matrix metalloproteinases (MMPs) to degrade ECM components, or promotion of liver tissue remodeling through angiogenic factor regulation.

To address these questions, this study utilized electrospinning to fabricate RSF scaffolds loaded with HGF and FGF-4. Preliminary results indicated that this functional RSF scaffold was capable of releasing approximately 3.6% of HGF and 2.7% of FGF-4 per day *in vitro* over a 16-day period, with sustained release thereafter.[16] Following implantation in a chronic hepatic fibrosis mouse model, systematic evaluation revealed that the RSF/HGF/FGF-4 scaffold significantly improved liver function, as indicated by serum biochemical analysis, and effectively reversed fibrotic architecture, as evidenced by histological assessment (H&E and Masson's trichrome staining). Furthermore, immunohistochemical staining showed that the scaffold uniquely promoted the concurrent formation of functional nascent vasculature (CD34+/ERG+) and biliary structures (MUC-1+/CK19+) at the implantation site. Mechanistically, transcriptomic sequencing and quantitative PCR analysis revealed that these therapeutic effects stem from a dual regulatory mechanism mediated by sustained growth factor release—simultaneously upregulating regenerative pathways such as bile secretion while downregu-

lating key inflammatory and fibrotic signaling pathways including NF-κB. In summary, this work not only validates the therapeutic potential of the RSF/HGF/FGF-4 scaffold in chronic liver fibrosis but also systematically elucidates its capacity to orchestrate multidimensional tissue repair through the temporal regulation of the hepatic microenvironment (Fig. 1).

2. Materials and methods

2.1. Establishment of the hepatic fibrosis model

The 6 to 8-week-old male BALB/c mice (SPF biotechnology, China) were used to conduct animal experiments. Mice were purchased from the Experimental Animal Center of the Academy of Military Medical Sciences (Beijing, China). All procedures were approved by the Animal Ethics Committee of the Chinese PLA General Hospital and conducted in strict accordance with the institutional guidelines for the care and use of laboratory animals. To induce chronic hepatic fibrosis, mice received intraperitoneal injections of 40% CCl_4 diluted in olive oil at a dose of 2 mL kg^{-1}, three times per week for 6–8 weeks.[17]

2.2. Preparation of RSF and RSF/HGF/FGF-4 scaffolds

RSF aqueous solutions at concentrations of 20 wt% and 33 wt% were prepared following previously reported protocols.[19] To prevent gelation of the high-concentration RSF solutions under neutral pH, all preparation and handling steps were performed at 4–8 °C. Specifically, when the concentration exceeded 15 wt%, the solution was promptly transferred to a shaker (HS 260 basic, IKA, Germany) and concentrated gently and uniformly at 120 rpm under cold airflow (4–8 °C) to minimize the risk of premature gelation. For electrospinning, aluminum foil was used as the fiber collector, placed 20 cm from a nozzle with an inner diameter of 0.6 mm. The electrospinning parameters were set to a flow rate of 1.1 mL h^{-1} and a voltage of 20 kV. RSF scaffolds were obtained after 3 hours of spinning.

Sterile lyophilized HGF and FGF-4 were purchased from Shanghai XinYu Biotechnology Co., Ltd (China). The growth factors were first reconstituted in phosphate-buffered saline (PBS, Gibco, USA) to a concentration of 1 mg mL^{-1}, then diluted in 0.1 wt% bovine serum albumin (BSA, Sigma-Aldrich, USA) solution to a final concentration of 0.625 mg mL^{-1}. A total of 520 μL of HGF solution and 440 μL of FGF-4 solution were mixed with 18 mL of 20 wt% RSF solution. After concentration, a 33 wt% RSF/HGF/FGF-4 spinning solution was obtained. Electrospinning of the RSF/HGF/FGF-4 scaffolds followed the same parameters as for the RSF-only scaffolds. Final post-treatment was carried out under mild conditions (37 °C, 90% relative humidity) to improve the water-insolubility of the RSF fibers.
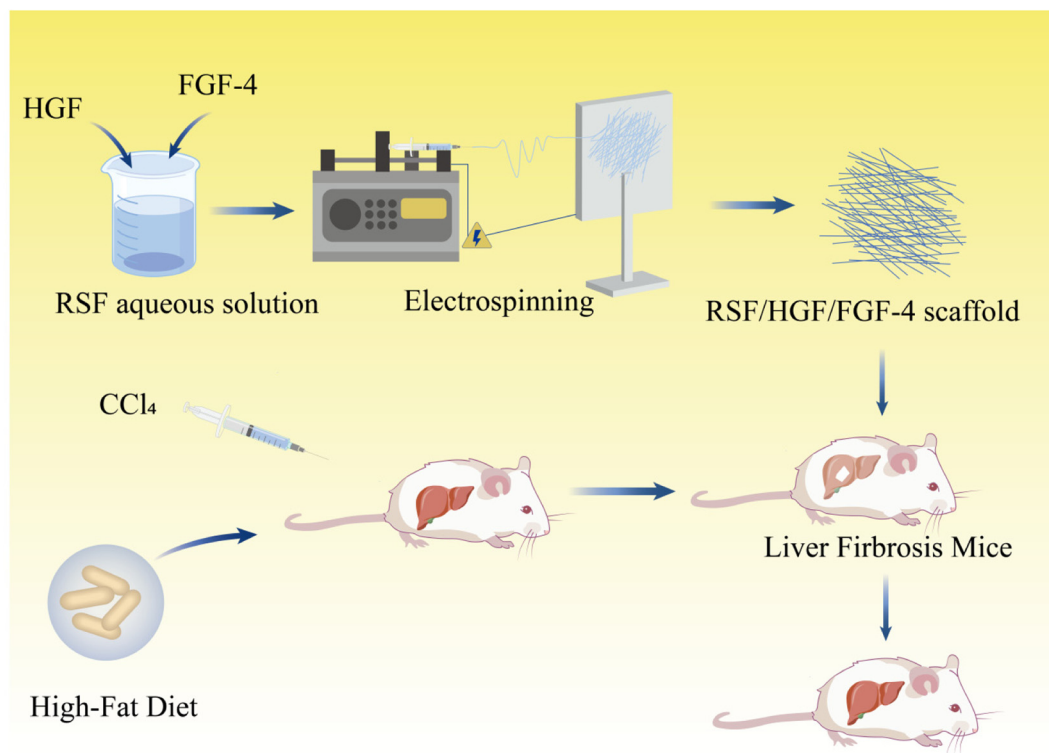
Fig. 1 Schematic diagram of the research. This schematic workflow showed the preparation process of RSF nanofiber scaffolds with sustained dual release of growth factors by electro-spinning, and investigation of the effects of the scaffolds in treating liver fibrosis of mice.

2.3. Transplantation and samples collection

Surgical procedures were performed as previously described.[20] Briefly, fibrotic mice were anesthetized *via* intraperitoneal injection of pentobarbital. The left lateral hepatic lobe was exposed, and the scaffold material was sutured and fixed onto the liver surface. The abdominal incision was then closed in layers according to standard surgical techniques. Serum and liver tissue samples were collected on day 7, 14, and 30 after transplantation, with $n = 3$ mice per group per time point.

2.4. Serological analysis of mice

To monitor dynamic changes in liver function, a fully automated biochemical analyzer (Mindray BS-240 Vet, China) was used to assess serum biomarkers, including alanine aminotransferase (ALT), aspartate aminotransferase (AST), alkaline phosphatase (ALP), albumin (ALB), total bilirubin (TBIL), triglycerides (TG), and total cholesterol (TC). Serum levels of the inflammatory marker C-reactive protein (CRP) were also measured using the same analyzer.

2.5. H&E staining and Masson's trichrome staining

To assess pathological changes in the liver during the experiment, H&E staining was performed to evaluate hepatic steatosis, hepatocellular necrosis, inflammatory cell infiltration, and fibrosis. In parallel, Masson's trichrome staining was used to assess the degree of liver fibrosis. Histological injury was eval-

uated using the SAF scoring system (steatosis, activity, fibrosis) by experienced pathologists from our hospital. Detailed scoring criteria are provided in Table S1 in the appendix.[21]

2.6. Immunohistochemical staining

Frozen liver tissue samples were rehydrated and fixed in 4% paraformaldehyde. After quenching endogenous peroxidase activity, tissues were blocked with PBS containing 5% goat serum and 2% BSA. Primary antibodies were applied and incubated overnight at 4 °C: anti-CD34 (Abcam, UK) and anti-ERG (Abcam, UK) for vascular marker detection, and anti-MUC (Abcam, UK) and anti-cytokeratin 19 (CK19; Abcam, UK) for bile duct identification. The following day, sections were incubated with secondary antibodies at room temperature for 1 hour, developed using 3,3′-diaminobenzidine (DAB), and counterstained with hematoxylin. Slides were sealed with neutral resin after dehydration in xylene and photographed using a microscope (Nikon, Japan). Each group included $n = 3$ samples.

2.7. Reverse transcription polymerase chain reaction (RT-PCR)

On day 7, RNA was extracted from liver tissue using TRIzol reagent (Invitrogen Life Technologies), and reverse transcription was performed to synthesize cDNA under the following conditions: 50 °C for 15 min and 85 °C for 5 s. The resulting cDNA was stored at 4 °C for subsequent quantitative PCR ana-

lysis. PCR conditions were as follows: initial denaturation at 95 °C for 30 s, denaturation at 95 °C for 10 s, and extension at 60 °C for 30 s, for a total of 40 cycles. Reactions were performed in triplicate, and relative expression levels were calculated using the 2−ΔΔCt method with actin as the internal control. Gene expression levels of TRAF2, Bax, FXR, and OAT in liver tissue were quantified. Primer sequences are listed in Table S2.

2.8. mRNA transcriptome sequencing analysis

Liver tissues were collected on day 7 post-scaffold transplantation, immediately frozen, and stored at −80 °C. Total RNA was extracted using TRIzol reagent or commercial RNA extraction kits, and RNA concentration, purity, and integrity were assessed using a NanoDrop spectrophotometer and Bioanalyzer. mRNA was enriched using poly(A) selection or ribosomal RNA depletion and then reverse-transcribed to cDNA. Library construction included cDNA fragmentation, end repair, A-tailing, adaptor ligation, PCR amplification, and purification. High-throughput sequencing was performed on an Illumina NovaSeq 6000 or HiSeq 4000 platform with appropriate read length and depth. Raw data quality was assessed using FastQC, and reads were trimmed using Trimmomatic or Cutadapt. Clean reads were aligned to the reference genome using HISAT2 or STAR, gene expression was quantified with HTSeq or featureCounts, and differential expression analysis was conducted using DESeq2 or edgeR. Differentially expressed genes were further subjected to Gene Ontology (GO) and Kyoto Encyclopedia of Genes and Genomes (KEGG) pathway enrichment analysis.

2.9. Statistical analysis

Data comparisons between groups were conducted using Student's t-test, following a normality test check. Statistical analyses were performed using GraphPad Prism 9 software (GraphPad Software Inc., San Diego, USA). Data are presented as mean ± standard deviation (SD), and p < 0.05 was considered statistically significant.

3. Result

3.1. Establishment of chronic liver fibrosis mice model

To validate the hepatic fibrosis model, a systematic pathological assessment was performed on day 56 post-induction. Gross examination revealed that normal livers displayed a uniform dark reddish-brown color, soft texture, and smooth surface. In contrast, livers from fibrotic mice appeared yellowish-brown with hardened texture, rough surface, and granular nodules (Fig. 2a). H&E staining showed that hepatic lobular architecture in fibrotic mice was deformed or even obliterated, accompanied by inflammatory cell infiltration and intracellular lipid droplet accumulation (Fig. 2b). Masson's trichrome staining revealed disorganized lobular structures and pronounced proliferation of blue-green fibrous tissue, forming thick fibrous bundles or reticular networks (Fig. 2c). SAF

scoring indicated a total score of 10 in the model group (Fig. 2d), signifying significant fibrotic lesions consistent with diagnostic criteria for hepatic fibrosis. These pathological findings confirmed the successful establishment of a chronic hepatic fibrosis mouse model for this study.

3.2. Biocompatibility of RSF/HGF/FGF-4 scaffolds in the liver fibrosis animal model

To assess the biocompatibility of the scaffolds, RSF/HGF/FGF-4 scaffolds were implanted onto the liver surface of fibrotic mice (Fig. 3a and b). Over the 30-day post-transplantation period, the scaffold–liver interface exhibited progressive integration. On day 7, the interface boundary was well defined, and tissue adherence to the scaffold was limited. By day 30, the scaffold was tightly integrated with liver tissue, with substantial neotissue proliferation and seamless fusion (Fig. 3c).

H&E staining revealed a large number of inflammatory cells surrounding the scaffold–liver interface on day 7. By day 30, inflammatory cell infiltration had notably decreased, and the interface appeared stabilized (Fig. 3d). These observations indicate that the RSF/HGF/FGF-4 scaffold is well tolerated by liver tissue and provides a reliable structural basis for therapeutic application. The dynamic integration process demonstrates the scaffold's favorable tissue compatibility in the fibrotic hepatic microenvironment.

3.3. Pathological study on the effects of RSF/HGF/FGF-4 in reversing liver fibrosis of mice model

To investigate the potential of the RSF scaffold in reversing hepatic fibrosis, Masson's trichrome staining and reticulin fiber analysis were performed on liver tissues collected at day 7, 14, and 30 post-transplantation (Fig. 4a and b). The extent of hepatic fibrosis gradually improved in both the RSF and RSF/HGF/FGF-4 groups over time. On day 7, lobular structures in all groups remained indistinct, with extensive fibrous tissue proliferation observed in the control and RSF groups. Blue-green fibrous bundles were evident around the portal areas and hepatic sinusoids, forming bundled or reticular structures. From day 14 to day 30, the RSF/HGF/FGF-4 group exhibited significantly reduced bundle thickness and density compared to the control group, accompanied by decreased fibrotic area and weakened staining intensity (P < 0.01 on day 14; P < 0.001 on day 30). By day 30, most fibrous bundles in the RSF and RSF/HGF/FGF-4 groups had been replaced by regenerating hepatic tissue, indicating marked fibrosis regression and tissue repair. These findings suggest a time-dependent reduction in fibrotic severity, decreased fibrous tissue distribution, and progressive restoration of hepatic lobular architecture following RSF/HGF/FGF-4 scaffold implantation.

3.4. Pathological study on the effects of RSF/HGF/FGF-4 on hepatic steatosis and inflammation

To further assess hepatic steatosis, H&E staining (Fig. 5a) and SAF scoring (Fig. 5b) were performed on liver tissues collected on day 7, 14, and 30 post-transplantation. On day 7, the RSF/HGF/FGF-4 group exhibited significantly less hepatocellular
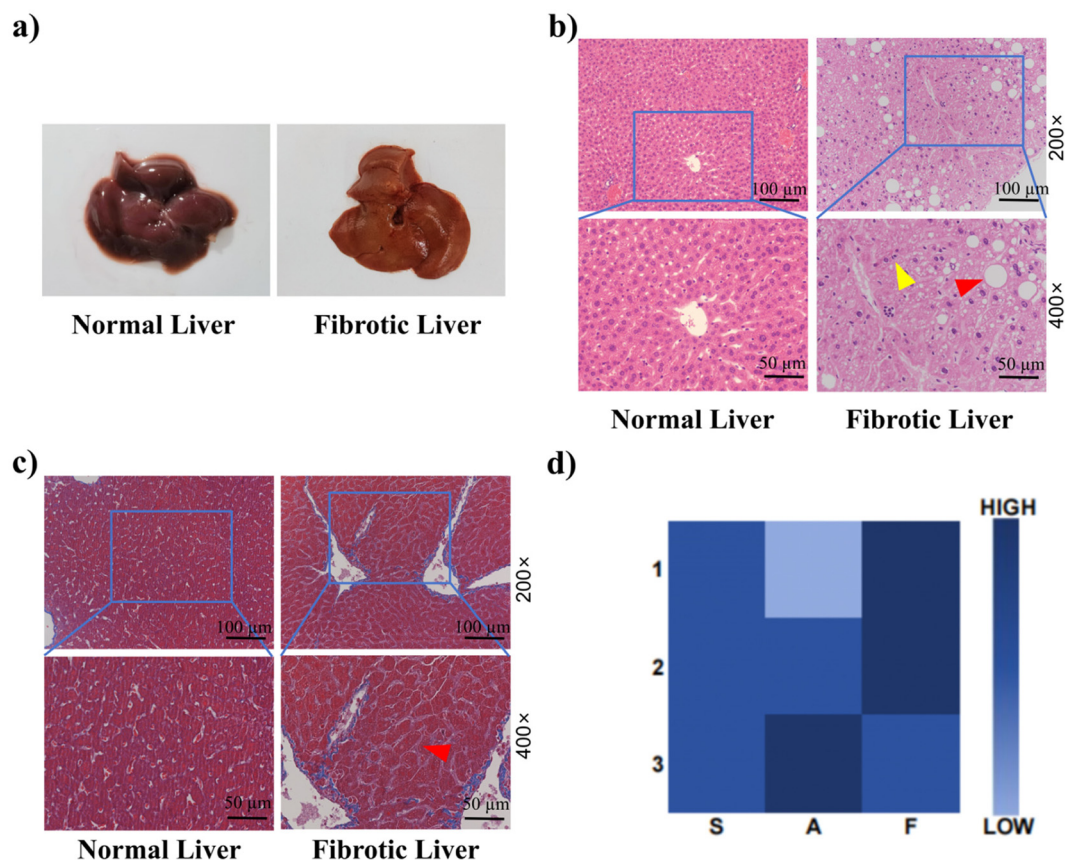
Fig. 2 Hepatic features of chronic liver fibrosis (CLF) mice. (a) Gross morphology of normal liver and liver after 56 days of intraperitoneal CCl$_4$ injection combined with high-fat diet. (b) H&E staining of normal liver and liver from CLF mice on day 56 (red arrows: lipid droplets; yellow arrows: inflammatory cells). (c) Masson's trichrome staining of normal and fibrotic liver tissue on day 56 (red arrows: fibrous bundles). (d) SAF scoring, $n = 3$.

ballooning, steatosis, inflammation, and focal necrosis than both the control and RSF-only groups. By day 14, macrovesicular steatosis was markedly reduced in the RSF/HGF/FGF-4 group, while steatosis remained prominent in the control group and was only moderately alleviated in the RSF group. By day 30, hepatocytes in the RSF/HGF/FGF-4 group appeared normal in size, with no evident inflammation or steatosis, whereas the control group still showed signs of inflammation, mild steatosis, and necrosis. SAF scores were significantly lower in the RSF/HGF/FGF-4 group than in the control group from day 7 onward ($P < 0.01$), reaching the lowest levels by day 30 ($P < 0.01$). Additionally, the RSF/HGF/FGF-4 group had significantly better scores than the RSF group on both day 7 and day 14 (*P* < 0.05). These results indicate that the combined application of RSF with HGF and FGF-4 markedly attenuates hepatic inflammation and steatosis, promoting tissue regeneration and demonstrating excellent biocompatibility and therapeutic efficacy.

3.5. Dynamic changes of biomarkers of liver function and the inflammatory after scaffold transplantation

To evaluate liver function over time, serum biochemical analyses were performed on days 7, 14, 30, and 60 post-implan-

tation. Results showed a progressive improvement in liver function markers (ALB, ALT, AST, ALP, TBIL, TC, TG) from the control group to the RSF/HGF/FGF-4 group, with the RSF/HGF/FGF-4 group showing the most significant improvement ($P < 0.01$ for ALB, ALT, AST, TBIL; $P < 0.001$ for ALP, TC, TG) (Fig. 6). The inflammatory marker CRP decreased steadily within 7 days post-implantation and reached its lowest level by day 30. The RSF/HGF/FGF-4 group exhibited a significantly greater reduction in CRP levels than the other groups ($P < 0.001$).

3.6. Observation of vascular and biliary system in RSF scaffold after transplantation by immunohistochemical staining

To examine neovascularization and biliary duct formation in liver tissue, immunohistochemistry was performed on day 14 post-transplantation. The expression of vascular markers (CD34 and ERG) and biliary duct markers (MUC-1 and CK19) confirmed the formation of new blood vessels and bile ducts were only observed in the RSF/HGF/FGF-4 group (Fig. 7). In the CD34 and ERG stained sections, red arrows indicate neovessels; in the MUC-1 and CK19 images, red arrows highlight newly formed bile ducts. In contrast, such organized, positive-
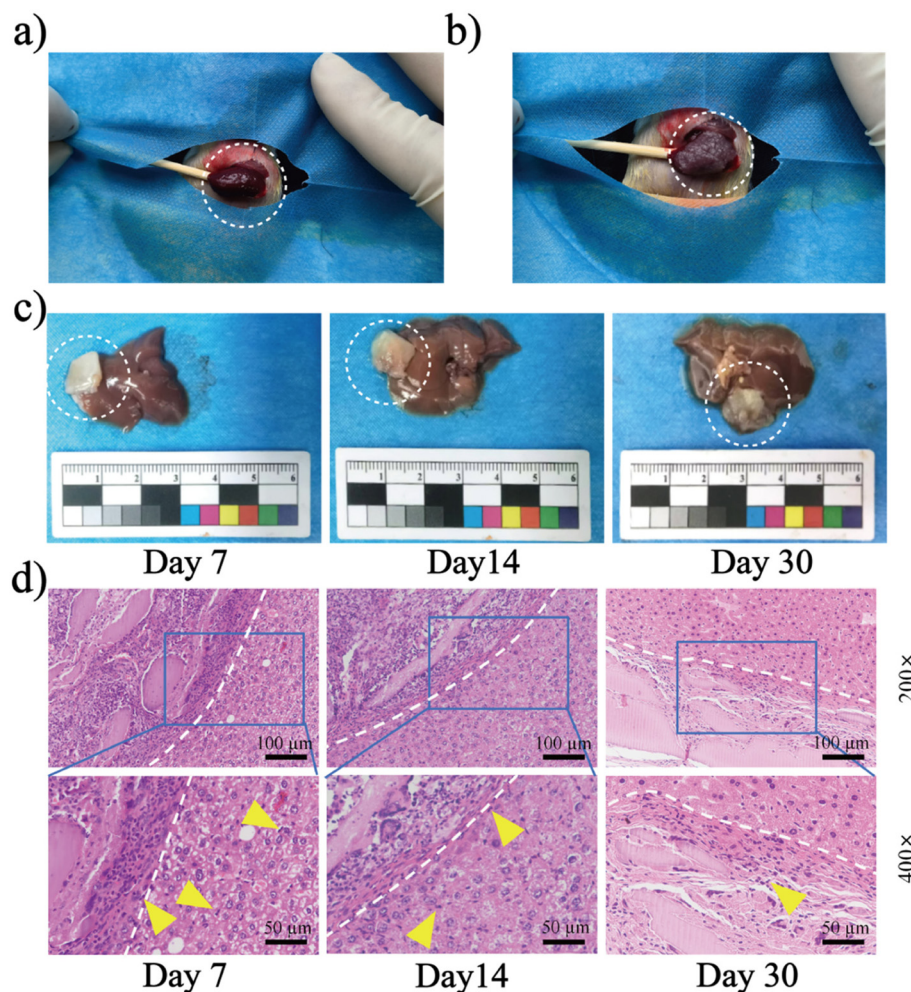
Fig. 3 The RSF scaffold exhibits favorable biocompatibility. (a) Gross morphology of mouse liver prior to surgery. (b) Intraoperative image showing RSF/HGF/FGF-4 scaffold adhered to the liver surface. (c) Gross appearance of liver–scaffold integration on postoperative days 7, 14, and 30. (d) H&E staining at the liver–scaffold interface on days 7, 14, and 30 (yellow arrows: inflammatory cells; white dashed line: interface of liver tissue and scaffold).

staining structures were not detected in the corresponding areas of the Control or RSF groups. These findings demonstrate that the RSF/HGF/FGF-4 scaffold promotes the formation of vascular- and biliary-like structures.

3.7. RNA transcriptome analysis of genes expressions involved in RSF scaffolds in reversing liver fibrosis

To explore the underlying mechanisms, transcriptome sequencing was conducted to assess differentially expressed genes. Compared with the control group, the RSF group exhibited 1916 differentially expressed genes, while the RSF/HGF/FGF-4 group had 1496 (Fig. 8a). Hierarchical clustering analysis revealed distinct gene expression profiles in the RSF/HGF/FGF-4 group compared with both the RSF and control groups (Fig. 8b).

KEGG pathway enrichment analysis (Fig. 8c) showed that the RSF/HGF/FGF-4 group significantly upregulated pathways related to cell proliferation, energy metabolism, bile secretion,

immune response, and cell migration—especially pathways involved in cholangiogenesis, bile acid transport, and lipid metabolism. In contrast, the RSF/HGF/FGF-4 group showed marked downregulation of pathways associated with immune responses, inflammation, cell adhesion, and fatty acid metabolism. For example, the NF-κB signaling pathway, known to play a central role in hepatic inflammation and fibrosis, was significantly suppressed. These results suggest that the RSF/HGF/FGF-4 scaffold may alleviate liver inflammation and fibrosis by modulating these molecular pathways, thereby promoting hepatic repair and regeneration.

3.8. Differential expressed genes in pathway of bile secretion signaling and NF-κB signaling were investigated by qPCR

To validate transcriptomic findings, RT-PCR was performed on selected differentially expressed genes. Compared with the RSF group, the RSF/HGF/FGF-4 group showed significantly elevated expression of FXR and OAT, key genes in the bile secretion
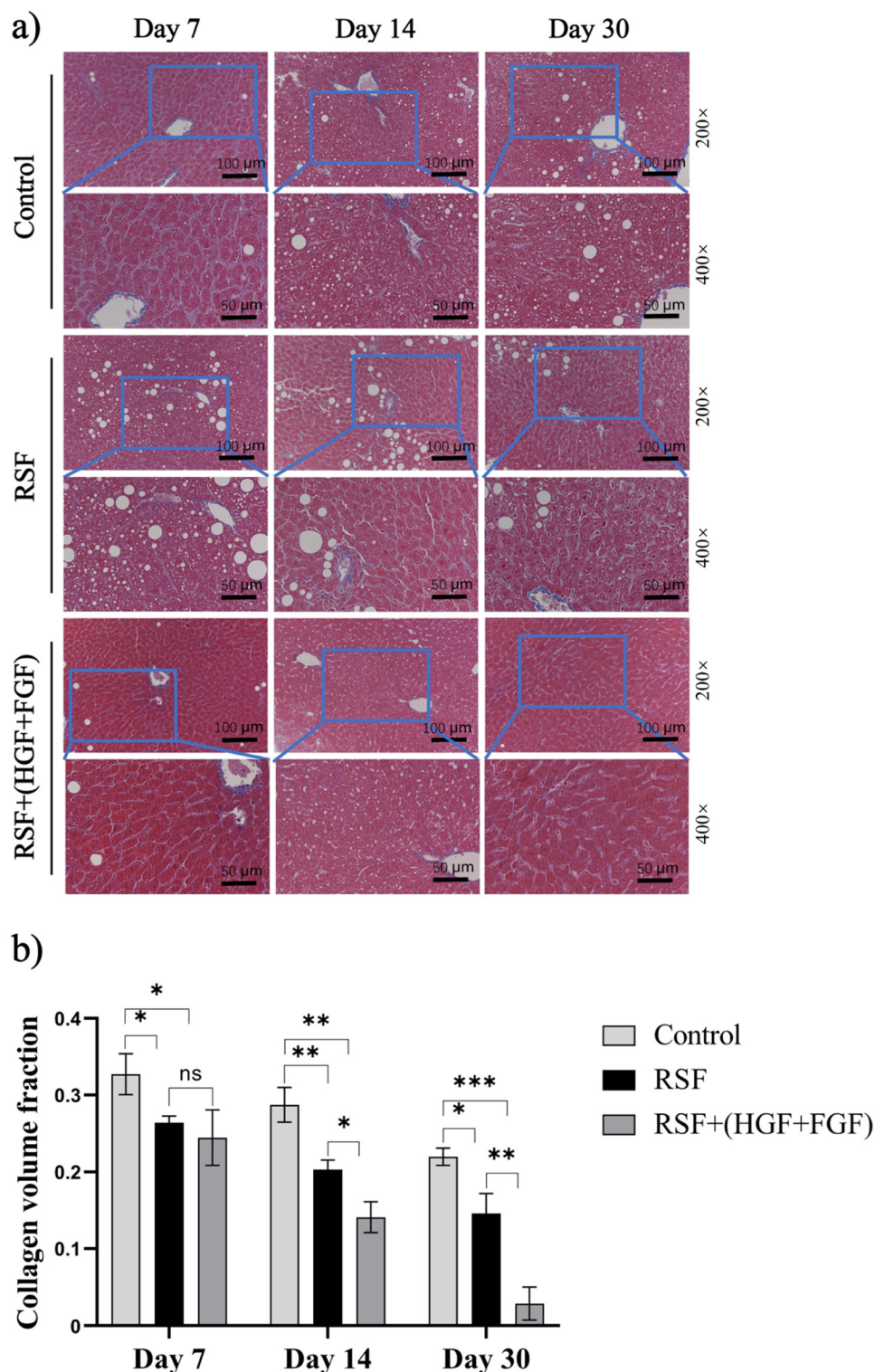
Fig. 4 Masson's trichrome staining and quantification of collagen area in transplanted livers. (a) Representative Masson's trichrome staining in each group on days 7, 14, and 30 post-transplantation. (b) Quantification of collagen area based on trichrome staining. All data is presented as mean $\pm$ SD (n = 3). Statistical analysis: *$P < 0.05$, **$P < 0.01$, ***$P < 0.001$, ****$P < 0.0001$, ns: not significant.

pathway ($P < 0.001$ and $P < 0.0001$, respectively). These genes are involved in bile acid synthesis and cellular transport. Conversely, genes in the NF-κB inflammatory pathway, includ-

ing TRAF2 and Bax, were significantly downregulated in the RSF/HGF/FGF-4 group ($P < 0.01$ and $P < 0.0001$, respectively), both of which are associated with immune activation and
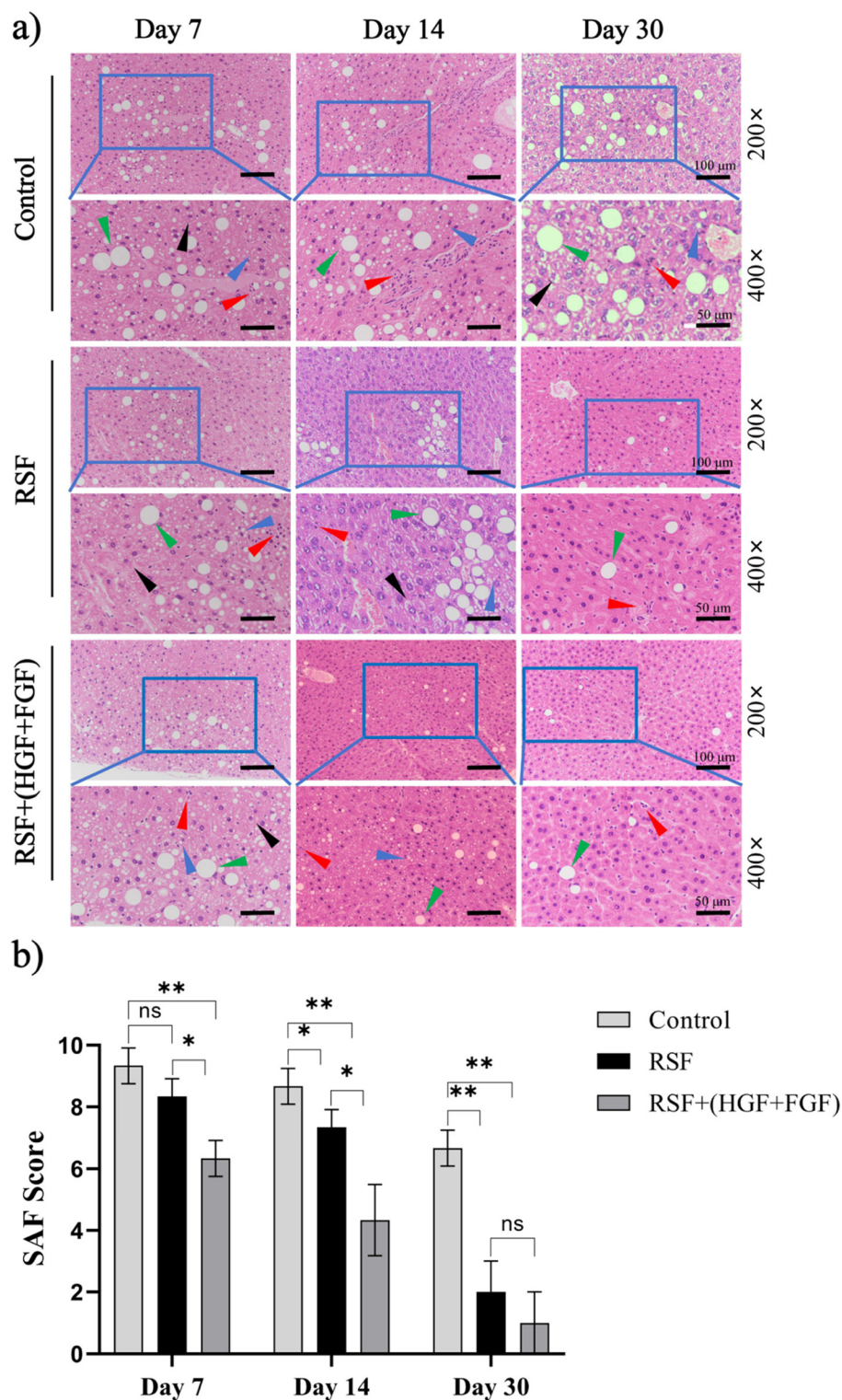
Fig. 5 H&E staining analysis of transplanted liver tissue. (a) Representative H&E staining of liver sections from each group on days 7, 14, and 30 post-transplantation (blue arrows: hepatocyte steatosis; green arrows: macrovesicular steatosis; red arrows: inflammatory cells; black arrows: ballooning degeneration). (b) SAF scoring table. All data is presented as mean $\pm$ SD (n = 3). Statistical analysis: *P < 0.05, **P < 0.01, ***P < 0.001, ****P < 0.0001, ns: not statistically significant.
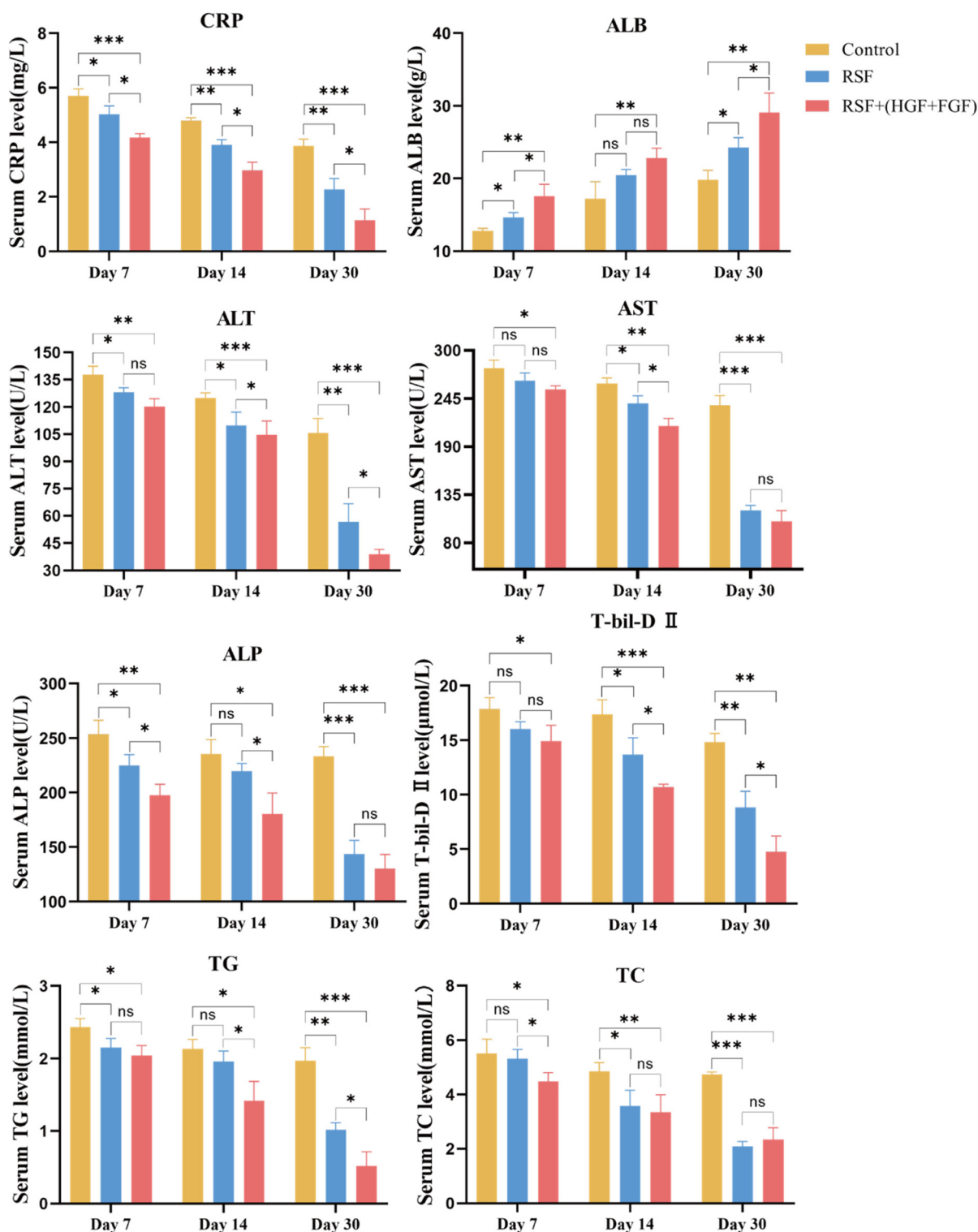
Fig. 6 Liver function and inflammatory marker analysis in CLF mice after transplantation. Levels of alanine aminotransferase (ALT), albumin (ALB), alkaline phosphatase (ALP), aspartate aminotransferase (AST), total bilirubin (Tbil), total cholesterol (TC), triglycerides (TG), and C-reactive protein (CRP) across different groups. All data is presented as mean ± SD (*n* = 3). Statistical analysis: *P < 0.05, **P < 0.01, ***P < 0.001, ****P < 0.0001, ns: not significant.
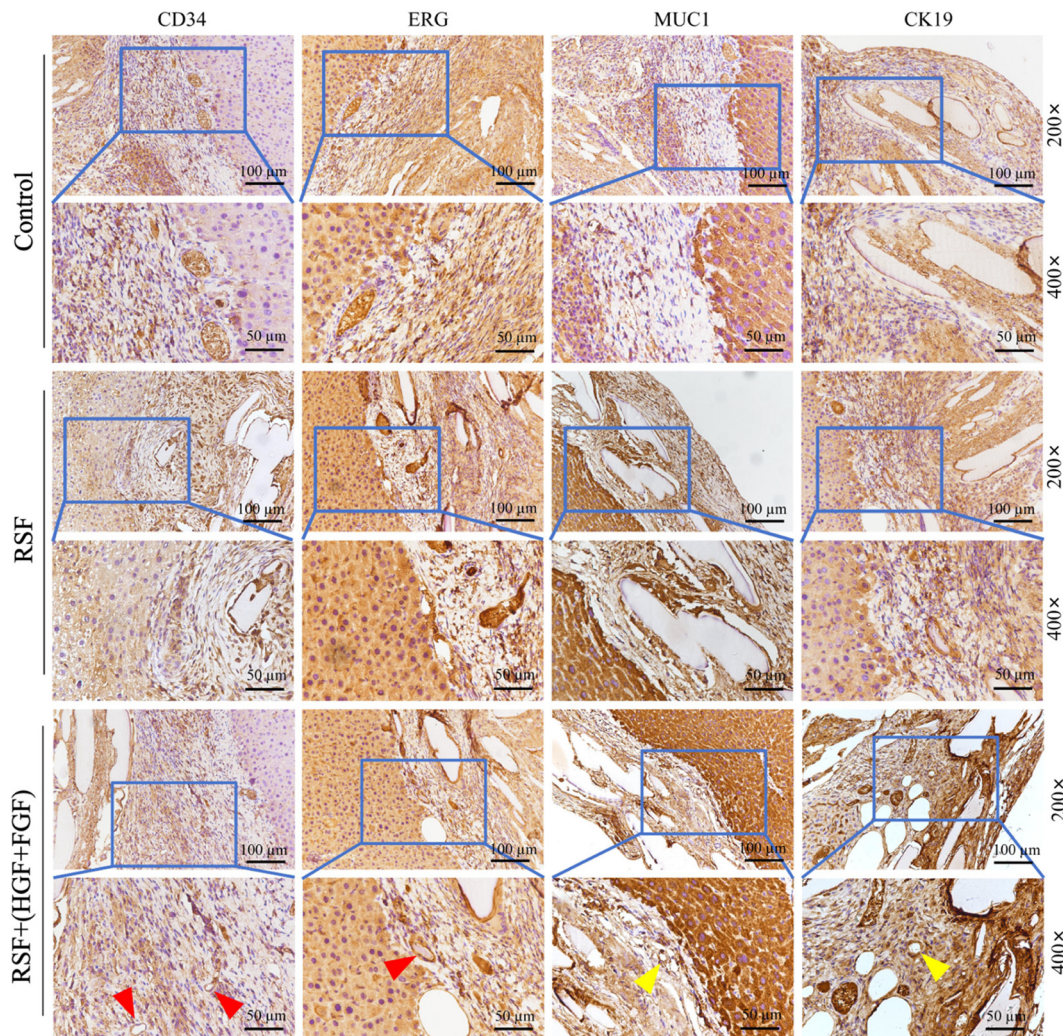
Fig. 7 Immunohistochemical staining result. Immunohistochemical staining of vascular markers CD34 and ERG (red arrows: blood vessels), and biliary duct markers MUC-1 and CK19 (yellow arrows: bile ducts) in each group.

apoptosis. These findings provide further mechanistic evidence for the antifibrotic effects of RSF/HGF/FGF-4 scaffolds (Fig. 9).

4. Discussion

The RSF/HGF/FGF-4 scaffold developed in this study demonstrated a marked antifibrotic effect in a liver fibrosis model through the sustained release of dual growth factors, and successfully induced the formation of neo-bile ducts. Transcriptomic analysis revealed a dual mechanism of action: activation of the bile secretion pathway promoted biliary morphogenesis, while inhibition of the NF-κB signaling cascade and mitochondria-dependent apoptosis exerted antifibrotic effects. This cell-free therapeutic strategy enables functional liver regeneration without the need for exogenous cell implan-

tation, thereby overcoming key limitations of conventional cell-based therapies, such as low engraftment efficiency and high cell mortality in clinical applications.[22,23]

Mechanistically, the synergistic action of HGF and FGF-4 forms a triple regulatory network encompassing antifibrosis, differentiation, and matrix remodeling. HGF activates the c-Met signaling cascade, triggering the PI3K/Akt and MAPK/ERK pathways to promote hepatic stem cell proliferation and enhance cell survival.[11,24] Concurrently, FGF-4 acts *via* the FGFR4–Ca^{2+}–CaMKKβ–AMPK axis to suppress TGF-β1/Smad3-mediated hepatic stellate cell activation and reduce Caspase-6-induced hepatocyte apoptosis.[25] In addition, both factors collaboratively block the TGF-β1/Smad3 fibrotic pathway *via* Akt, and jointly enhance MMP-9 activity to remodel collagen deposition,[26–28] thus achieving multidimensional intervention in the fibrotic hepatic microenvironment. It is worth noting that most existing studies are limited to *in vitro* experiments or
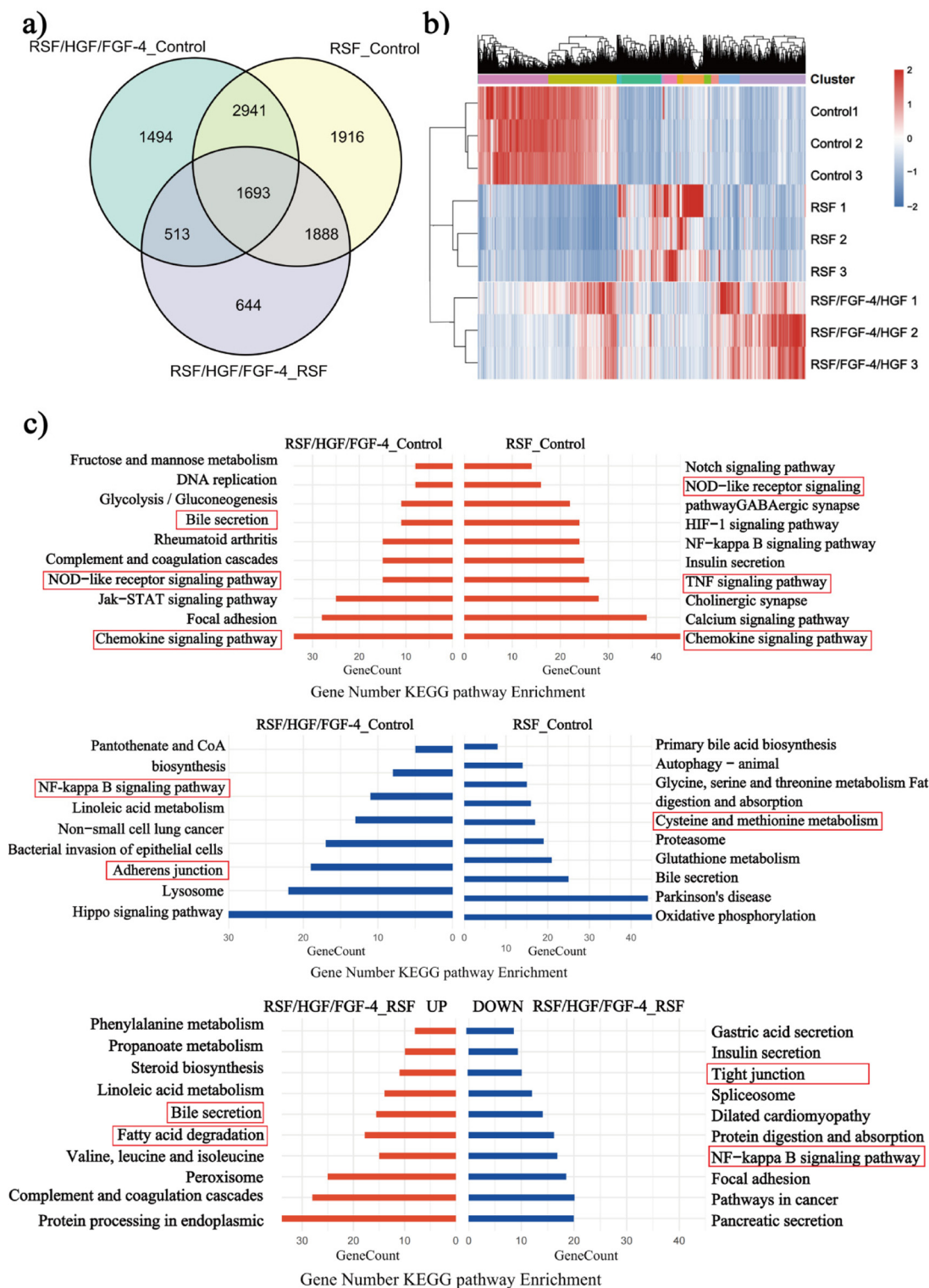
Fig. 8 RNA sequencing after scaffold transplantation. (a) Venn diagram showing differentially expressed genes (DEGs) among the groups. (b) Hierarchical clustering of DEG expression levels displayed as heatmaps. (c) KEGG pathway analysis of significantly upregulated and downregulated pathways. Red boxes indicate pathways related to immune-inflammatory regulation and metabolic modulation during liver regeneration.

in vivo models lacking integration with biomaterials. The short half-lives of free cytokines hinder their capacity to sustain liver repair *in vivo*. The RSF/HGF/FGF-4 system developed in this study, leveraging the controlled-release properties of the silk fibroin scaffold, was shown *in vitro* to release 3.6% HGF and 2.7% FGF-4 per day over a period of 16 days.[16] This sustained
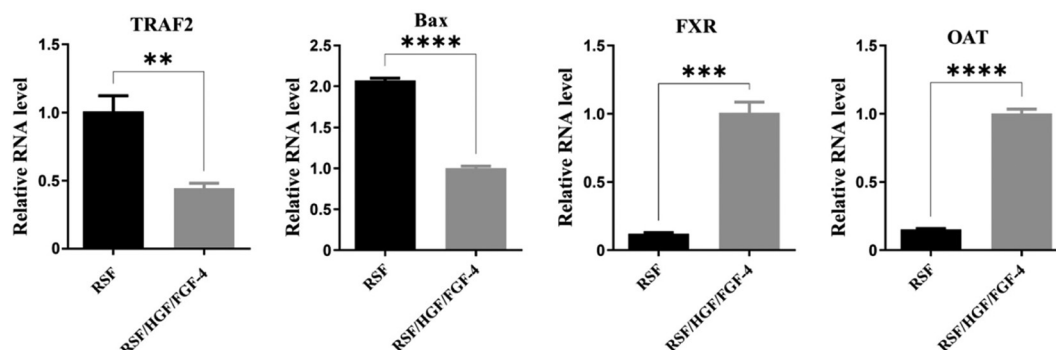
Fig. 9 RT-PCR analysis of relative RNA expression levels of TRAF2, Bax, FXR, and OAT in RSF and RSF/HGF/FGF-4 groups. Compared with the RSF group, TRAF2 and Bax were significantly downregulated, while FXR and OAT were significantly upregulated in the RSF/HGF/FGF-4 group. All data is shown as mean ± SD (n = 3). Statistical analysis: *P < 0.05, **P < 0.01, ***P < 0.001, ****P < 0.0001, ns: not significant. These findings demonstrate significant differences between the RSF and RSF/HGF/FGF-4 groups.

release profile is markedly superior to the burst release (>65% within 3 days) observed in PLGA microspheres and the mechanical instability of alginate hydrogels,[29,30] laying a solid foundation for long-acting growth factor therapy *in vivo*.

In addition to its molecular synergism, the material properties of the silk fibroin scaffold provide essential support for its therapeutic efficacy. Its controlled release kinetics prevent the bioavailability decline associated with rapid degradation in traditional carriers, while optimized pore size design inhibits nonspecific proliferation of fibroblasts, thereby reducing pro-fibrotic risk. Compared with 3D-printed scaffolds or decellularized liver matrices, which can mimic hepatic structure but fail to maintain long-term function,[31,32] the RSF/HGF/FGF-4 system integrates dynamic growth factor delivery with material stability to promote simultaneous neogenesis of bile ducts and blood vessels within a fibrotic hepatic environment. Immunohistochemical results demonstrated that this system successfully induces functional neo-biliary and neo-vascular structures *in vivo*, whereas conventional VEGF-based therapies are hindered by the short half-life of VEGF, leading to dysfunctional neovasculature,[33] and most studies on biliary morphogenesis remain confined to *in vitro* settings.[34,35] These findings highlight the translational potential and breakthrough advances achieved by the RSF/HGF/FGF-4 system in *in vivo* tissue reconstruction.

To further validate the transcriptomic findings, RT-PCR was selectively performed on key differentially expressed genes. The results confirmed that the scaffold exerts a dual regulatory effect by coordinately modulating the FXR-OAT and NF-κB-TRAF2/Bax signaling axes: upregulating FXR and OAT to enhance bile acid metabolism and biliary differentiation, while downregulating TRAF2 and Bax to suppress inflammatory cascades and reduce mitochondria-dependent apoptosis. HGF and FGF-4 activated MAPK/ERK and PI3K/Akt signaling cascades contribute to this coordinated regulation: on the one hand, FXR phosphorylation promotes OAT expression and activates the FXR-OSTα/β axis, thereby modulating biliary cell polarity and proliferation; on the other hand, inhibition of

TRAF2 activity and Bax mitochondrial translocation integrates anti-inflammatory and antifibrotic effects.

Although this study has demonstrated the therapeutic potential of the system, several scientific questions remain to be addressed. The precise mechanisms underlying the formation of neo-bile ducts and vasculature have yet to be fully elucidated, and the long-term functionality of these newly formed structures under physiological conditions requires further investigation. Future studies may employ single-cell sequencing to resolve lineage dynamics and incorporate long-term follow-up to evaluate the structural stability and integration of regenerated tissues. In summary, this cell-free therapeutic strategy based on the RSF scaffold combined with growth factors offers an innovative and translationally promising paradigm for liver regeneration and the treatment of chronic hepatic injury.

5. Conclusion

In this study, an RSF scaffold loaded with HGF, FGF-4 was implanted into a chronic liver fibrosis mouse model, resulting in marked improvements in liver function, attenuation of fibrosis, and the formation of neo-bile ducts and vasculature at the implantation site. Transcriptomic analysis further revealed that the scaffold promotes bile acid synthesis by upregulating the bile secretion signaling pathway, while inhibiting hepatic steatosis through downregulation of the NF-κB signaling pathway. Taken together, these findings demonstrate that the RSF/HGF/FGF-4 scaffold holds great promise as an ideal biomaterial for the treatment of liver fibrosis. This strategy provides an innovative and effective approach for hepatic disease therapy and lays a solid foundation for future advances in this field.

Author contributions

Jingyi Wang: writing – review & editing, writing – original draft, software, methodology, formal analysis, data curation.

Zhanbo Wang: validation, methodology, formal analysis, data curation. Shuo Zhao: software, methodology. Daxu Zhang: methodology, formal analysis, data curation. Weilong Li: methodology, formal analysis. Jingjing Hu: methodology. Shujun Ye: methodology. Xiaonan Shi: methodology. Xiaojiao Liu: methodology. Yaopeng Zhang: supervision. Li Yan: supervision, resources, funding acquisition, conceptualization.

Conflicts of interest

The authors have declared that no competing interests exist.

Data availability

Supplementary information (SI) is available. See DOI: https://doi.org/10.1039/d5bm01314c.

Acknowledgements

References

1 S. K. Asrani, H. Devarbhavi, J. Eaton and P. S. Kamath, Burden of liver diseases in the world, *J. Hepatol.*, 2019, **70**(1), 151–171.

2 H. Devarbhavi, S. K. Asrani, J. P. Arab, Y. A. Nartey, E. Pose and P. S. Kamath, Global burden of liver disease: 2023 update, *J. Hepatol.*, 2023, **79**(2), 516–537.

3 M. Zamani, S. Alizadeh-Tabari, V. Ajmera, S. Singh, M. H. Murad and R. Loomba, Global Prevalence of Advanced Liver Fibrosis and Cirrhosis in the General Population: A Systematic Review and Meta-analysis, *Clin. Gastroenterol. Hepatol.*, 2025, **23**(7), 1123–1134.

4 R. Melaram, Environmental Risk Factors Implicated in Liver Disease: A Mini-Review, *Front. Public Health*, 2021, **9**, 683719.

5 S. Tian, X. Zhou, M. Zhang, L. Cui, B. Li, Y. Liu, *et al.*, Mesenchymal stem cell-derived exosomes protect against liver fibrosis via delivering miR-148a to target KLF6/STAT3 pathway in macrophages, *Stem Cell Res. Ther.*, 2022, **13**(1), 330.

6 M. Yan, J. Yao, Y. Xie, P. Jiang, J. Yan and X. Li, Bioreactor-based stem cell therapy for liver fibrosis, *Biofabrication*, 2024, **16**(2), 025028.

7 L. Spahr, Y. Chalandon, S. Terraz, V. Kindler, L. Rubbia-Brandt, J. L. Frossard, *et al.*, Autologous bone marrow mononuclear cell transplantation in patients with decompensated alcoholic liver disease: a randomized controlled trial, *PLoS One*, 2013, **8**(1), e53719.

8 H. Liu, H. Huang, Y. Liu, Y. Yang, H. Deng, X. Wang, *et al.*, Adipose-derived mesenchymal stem cells inhibit hepatic stellate cells activation to alleviate liver fibrosis via Hippo pathway, *Stem Cell Res. Ther.*, 2024, **15**(1), 378.

9 H. Sun, R. E. Pratt, C. P. Hodgkinson and V. J. Dzau, Sequential paracrine mechanisms are necessary for the therapeutic benefits of stem cell therapy, *Am. J. Physiol.: Cell Physiol.*, 2020, **319**(6), C1141–C1150.

10 J. Ankrum and J. M. Karp, Mesenchymal stem cell therapy: Two steps forward, one step back, *Trends Mol. Med.*, 2010, **16**(5), 203–209.

11 Z. Cheng, L. Liu, X. J. Zhang, M. Lu, Y. Wang, V. Assfalg, *et al.*, Peroxisome Proliferator-Activated Receptor gamma negatively regulates liver regeneration after partial hepatectomy via the HGF/c-Met/ERK1/2 pathways, *Sci. Rep.*, 2018, **8**(1), 11894.

12 H. M. Hassan, O. Onabote, M. Isovic, D. T. Passos, F. A. Dick and J. Torchia, Regulation of Chromatin Accessibility by the Farnesoid X Receptor Is Essential for Circadian and Bile Acid Homeostasis In Vivo, *Cancers*, 2022, **14**(24), 6191.

13 X. Wang, C. Guo, L. Guo, M. Wang, M. Liu, Y. Song, *et al.*, Radially Aligned Porous Silk Fibroin Scaffolds as Functional Templates for Engineering Human Biomimetic Hepatic Lobules, *ACS Appl. Mater. Interfaces*, 2022, **14**(1), 201–213.

14 H. Wu, F. Xia, L. Zhang, C. Fang, J. Lee, L. Gong, *et al.*, A ROS-Sensitive Nanozyme-Augmented Photoacoustic Nanoprobe for Early Diagnosis and Therapy of Acute Liver Failure, *Adv. Mater.*, 2022, **34**(7), e2108348.

15 Y. Yang, Z. Yu, X. Lu, J. Dai, C. Zhou, J. Yan, *et al.*, Minimally invasive bioprinting for in situ liver regeneration, *Bioact. Mater.*, 2023, **26**, 465–477.

16 X. Liu, X. Shi, D. Zhang, S. Zhao, J. Hu, Q. Ouyang, *et al.*, Silk fibroin electrospun scaffolds with sustained dual release of growth factors enhance acute liver failure treatment, *Composites, Part B*, 2025, **296**, 112260.

17 W. Li, X. Shi, D. Zhang, J. Hu, S. Zhao, S. Ye, *et al.*, Adipose derived mesenchymal stem cell-seeded regenerated silk fibroin scaffolds reverse liver fibrosis in mice, *J. Mater. Chem. B*, 2025, **13**(13), 4201–4213.

18 L. Xu, S. Wang, X. Sui, Y. Wang, Y. Su, L. Huang, *et al.*, Mesenchymal Stem Cell-Seeded Regenerated Silk Fibroin Complex Matrices for Liver Regeneration in an Animal Model of Acute Liver Failure, *ACS Appl. Mater. Interfaces*, 2017, **9**(17), 14716–14723.

19 S. Fan, Y. Zhang, H. Shao and X. Hu, Electrospun regenerated silk fibroin mats with enhanced mechanical properties, *Int. J. Biol. Macromol.*, 2013, **56**, 83–88.

20 J. Hu, S. He, D. Zhang, Z. Wang, S. Zhao, X. Shi, *et al.*, Constructing liver-like tissue in situ based on plant-derived cellulose scaffolds alleviating acute liver injury, *Mater. Des.*, 2024, **240**, 112856.

21 P. Bedossa, Utility and appropriateness of the fatty liver inhibition of progression (FLIP) algorithm and steatosis, activity, and fibrosis (SAF) score in the evaluation of biop-

sies of nonalcoholic fatty liver disease, *Hepatology*, 2014, **60**(2), 565–575.

22 S. Baldari, G. Di Rocco, M. Piccoli, M. Pozzobon, M. Muraca and G. Toietta, Challenges and Strategies for Improving the Regenerative Effects of Mesenchymal Stromal Cell-Based Therapies, *Int. J. Mol. Sci.*, 2017, **18**(10), 2087.

23 G. E. Salazar-Noratto, G. Luo, C. Denoeud, M. Padrona, A. Moya, M. Bensidhoum, *et al.*, Understanding and leveraging cell metabolism to enhance mesenchymal stem cell transplantation survival in tissue engineering and regenerative medicine applications, *Stem Cells*, 2020, **38**(1), 22–33.

24 A. Sánchez and I. Fabregat, Growth factor- and cytokine-driven pathways governing liver stemness and differentiation, *World J. Gastroenterol.*, 2010, **16**(41), 5148–5161.

25 L. Song, L. Wang, Y. Hou, J. Zhou, C. Chen, X. Ye, *et al.*, FGF4 protects the liver from nonalcoholic fatty liver disease by activating the AMP-activated protein kinase-Caspase 6 signal axis, *Hepatology*, 2022, **76**(4), 1105–1120.

26 M. Kwiecinski, A. Noetel, N. Elfimova, J. Trebicka, S. Schievenbusch, I. Strack, *et al.*, Hepatocyte growth factor (HGF) inhibits collagen I and IV synthesis in hepatic stellate cells by miRNA-29 induction, *PLoS One*, 2011, **6**(9), e24568.

27 S. Kletukhina, G. Mutallapova, A. Titova and M. Gomzikova, Role of Mesenchymal Stem Cells and Extracellular Vesicles in Idiopathic Pulmonary Fibrosis, *Int. J. Mol. Sci.*, 2022, **23**(19), 11212.

28 A. Jazwa, P. Kucharzewska, J. Leja, A. Zagorska, A. Sierpniowska, J. Stepniewski, *et al.*, Combined vascular endothelial growth factor-A and fibroblast growth factor 4 gene transfer improves wound healing in diabetic mice, *Genet. Vaccines Ther.*, 2010, **8**, 6.

29 R. Mietzner, C. Kade, F. Froemel, D. Pauly, W. D. Stamer, A. Ohlmann, *et al.*, Fasudil Loaded PLGA Microspheres as Potential Intravitreal Depot Formulation for Glaucoma Therapy, *Pharmaceutics*, 2020, **12**(8), 706.

30 X. Chen, T. Wu, Y. Bu, H. Yan and Q. Lin, Fabrication and Biomedical Application of Alginate Composite Hydrogels in Bone Tissue Engineering: A Review, *Int. J. Mol. Sci.*, 2024, **25**(14), 7810.

31 J. S. Zhang, Z. B. Wang, Z. Z. Lai, J. W. Yang, W. J. Song, Y. B. Wei, *et al.*, Polyethylene glycol crosslinked decellularized single liver lobe scaffolds with vascular endothelial growth factor promotes angiogenesis in vivo, *Hepatobiliary Pancreatic Dis. Int.*, 2023, **22**(6), 622–631.

32 I. Matai, G. Kaur, A. Seyedsalehi, A. McClinton and C. T. Laurencin, Progress in 3D bioprinting technology for tissue/organ regenerative engineering, *Biomaterials*, 2020, **226**, 119536.

33 L. Yang, J. Kwon, Y. Popov, G. B. Gajdos, T. Ordog, R. A. Brekken, *et al.*, Vascular endothelial growth factor promotes fibrosis resolution and repair in mice, *Gastroenterology*, 2014, **146**(5), 1339–1350.

34 F. Sampaziotis, A. W. Justin, O. C. Tysoe, S. Sawiak, E. M. Godfrey, S. S. Upponi, *et al.*, Reconstruction of the mouse extrahepatic biliary tree using primary human extrahepatic cholangiocyte organoids, *Nat. Med.*, 2017, **23**(8), 954–963.

35 H. Thomas, Regenerative medicine: Bioengineering the common bile duct, *Nat. Rev. Gastroenterol. Hepatol.*, 2017, **14**(9), 504–505.